

A Closed-Loop Process for Rapid and Selective Lithium Extraction and Resynthesis from Spent LiFePO₄ Batteries

Author

Liu, Ruijing, Liu, Yuxiao, Li, Jianjiang, Chen, Yuanlin, Zhu, Yule, Zhang, Kunzheng, Zhao, Shuxian, Du, Liang, Zhu, Xiaoyi, Zhang, Lei

Published

2025

Journal Title

Molecules

Version

Version of Record (VoR)

DOI

[10.3390/molecules30122587](https://doi.org/10.3390/molecules30122587)

Rights statement

© 2025 by the authors. Licensee MDPI, Basel, Switzerland. This article is an open access article distributed under the terms and conditions of the Creative Commons Attribution (CC BY) license (<https://creativecommons.org/licenses/by/4.0/>).

Downloaded from


<https://hdl.handle.net/10072/437532>

Griffith Research Online

<https://research-repository.griffith.edu.au>

Article

A Closed-Loop Process for Rapid and Selective Lithium Extraction and Resynthesis from Spent LiFePO₄ Batteries

Ruijing Liu ^{1,2,†}, Yuxiao Liu ^{1,2,†}, Jianjiang Li ^{1,2}, Yuanlin Chen ³, Yule Zhu ^{1,2}, Kunzheng Zhang ^{1,2}, Shuxian Zhao ^{1,2}, Liang Du ⁴, Xiaoyi Zhu ^{1,2,*} and Lei Zhang ^{4,*} 

¹ College of Mechanical and Electrical Engineering, Qingdao University, Qingdao 266071, China; 13864223168@163.com (R.L.); jjli@qdu.edu.cn (J.L.); 13930175225@163.com (Y.Z.); 17861227940@163.com (K.Z.); 16716325866@163.com (S.Z.)

² School of Environment and Geography, College of Environmental Science and Engineering, Qingdao University, Qingdao 266071, China

³ Qingdao Grain & Oils Quality Inspection and Military Grain & Oils Supply Center, Qingdao 266042, China; chenyl4518@163.com

⁴ Centre for Catalysis and Clean Energy, Gold Coast Campus, Griffith University, Southport, QLD 4222, Australia; liang.du@griffithuni.edu.au

* Correspondence: xyzhu@qdu.edu.cn (X.Z.); lei.zhang@griffith.edu.au (L.Z.)

† These authors contributed equally to this work.

Abstract: The rapid growth of lithium iron phosphate (LiFePO₄, LFP)-based lithium-ion batteries in energy storage raises urgent challenges for resource recovery and environmental protection. In this study, we propose a novel method for rapid and selective lithium extraction and the resynthesis of cathodes from spent LFP batteries, aiming to achieve an economically feasible and efficient recycling process. In this process, a selective leaching H₂SO₄-H₂O₂ system is employed to rapidly and selectively extract lithium, achieving a leaching efficiency of 98.72% within just 10 min. Through an exploration of the precipitation conditions of the lithium-containing solution, high-purity Li₂CO₃ is successfully obtained. The recovered FePO₄ and Li₂CO₃ are then used to resynthesize LFP cathode materials through a carbon-thermal reduction method. A preliminary economic analysis reveals that the disposal cost of spent LFP batteries is approximately USD 2.63 per kilogram, while the value of regenerated LFP reaches USD 4.46, highlighting the economic advantages of this process. Furthermore, with an acid-to-lithium molar ratio of only 0.57—just slightly above the stoichiometric 0.5—the process requires minimal acid usage, offering clear environmental benefits. Overall, this work presents a green, efficient, and economically viable strategy for recycling spent LFP batteries, showcasing strong potential for industrial application and contributing significantly to the development of a circular lithium battery economy.

Keywords: LiFePO₄; spent lithium-ion batteries; leaching; recycling process; regeneration



Academic Editor: Sheng-Heng Chung

Received: 24 April 2025

Revised: 17 May 2025

Accepted: 10 June 2025

Published: 13 June 2025

Citation: Liu, R.; Liu, Y.; Li, J.; Chen, Y.; Zhu, Y.; Zhang, K.; Zhao, S.; Du, L.; Zhu, X.; Zhang, L. A Closed-Loop Process for Rapid and Selective Lithium Extraction and Resynthesis from Spent LiFePO₄ Batteries.

Molecules **2025**, *30*, 2587. <https://doi.org/10.3390/molecules30122587>

Copyright: © 2025 by the authors. Licensee MDPI, Basel, Switzerland. This article is an open access article distributed under the terms and conditions of the Creative Commons Attribution (CC BY) license (<https://creativecommons.org/licenses/by/4.0/>).

1. Introduction

In recent years, the rapid development of the electric vehicle industry and the large-scale deployment of renewable energy storage systems have led to explosive growth in the demand for lithium-ion batteries [1–3]. Among them, lithium iron phosphate (LFP) batteries have become the mainstream technology in the power battery sector due to their high safety, long cycle life, and low-cost advantages [4–6]. According to data from the China Automotive Battery Innovation Alliance, China's total power battery production reached 778.2 GWh in 2023, with LFP batteries accounting for 531.4 GWh, representing a dominant market share of 68.29%. Market research predicts that the global LFP battery

market will continue to expand at a compound annual growth rate of 6.39%, reaching USD 67.39 billion by 2029 [7]. However, as the first wave of commercial electric vehicles reaches their end-of-life cycle, it is estimated that 313,300 tons of spent LFP (SLFP) batteries will be generated globally by 2030. These retired batteries not only contain strategic resources such as lithium and phosphorus worth over CNY 20 billion but also pose environmental risks such as heavy metal pollution if improperly disposed [8–10]. Therefore, developing efficient and economical LFP battery recycling technologies has become a critical task for ensuring sustainable lithium supply and promoting the green development of the new energy industry [11].

Among the components of LFP batteries, the cathode material accounts for 36% of the total cost, making its efficient recycling crucial for both cost reduction and resource conservation [12,13]. Current cathode recycling technologies mainly revolve around three approaches: pyrometallurgy, hydrometallurgy, and direct regeneration [14–18]. Despite the simplicity of the pyrometallurgy process, it exhibits notable drawbacks including excessive energy consumption (exceeding 1000 °C), suboptimal metal recovery rates (Li < 50%), and a propensity to generate impurities such as $\text{LiFe}(\text{P}_2\text{O}_7)$, Fe_xP , and P_2O_5 , as well as dioxins [19,20]. Direct regeneration can maintain the structural integrity of the material but requires stringent purity standards (impurity content < 3%), making it unsuitable for complex material systems in real-world recycling scenarios [21–25]. In contrast, hydrometallurgy has become the mainstream approach due to its high metal recovery rates (Li > 95%) and process controllability [26–30]. However, traditional hydrometallurgical processes still face two major technical bottlenecks. First, the need for excessive inorganic acid (the molar ratio of $\text{H}_2\text{SO}_4/\text{Li}$ is 3.94 and the solid–liquid ratio is 100 g/L) results in significant wastewater generation. Secondly, the requirement for complex separation steps after the simultaneous leaching of iron and lithium significantly increases processing costs [31–33]. For example, Zheng et al. [34] achieved a 97.2% lithium leaching rate using a $2.5 \text{ mol L}^{-1} \text{ H}_2\text{SO}_4$ system, but the process required 4 h of reaction time and generated a large amount of iron-containing wastewater. Zhang et al. [28] developed a sodium citrate-assisted leaching process that controlled the iron leaching rate at 5.1%, but it required 5 h of ball-milling pretreatment and an additive dosage 10 times the stoichiometric ratio, rendering it economically unfeasible.

To address these technical challenges, this study innovatively constructed a short-process recycling system integrating “selective leaching, directional precipitation, and closed-loop regeneration” (Figure 1). Technical breakthroughs are reflected in the following aspects: First, a $\text{H}_2\text{SO}_4\text{-H}_2\text{O}_2$ collaborative leaching system was developed, which achieves the transformation of Fe^{2+} to Fe^{3+} by controlling the redox potential, simultaneously completing lithium leaching and iron–phosphorus fixation. This system enables selective lithium leaching (Li leaching rate > 98%, Fe leaching rate < 0.45%) within 10 min using near-stoichiometric acid, reducing reaction time by 95.8% and acid consumption by 85.53% compared to traditional processes [35,36]. Second, a pH gradient-controlled Li_2CO_3 directional precipitation model was established, which introduced a seed-induced growth mechanism to improve precipitation efficiency to 98.5% while controlling the mean particle size at 0.61 μm , making it directly usable for subsequent synthesis. Additionally, an innovative $\text{FePO}_4\text{-Li}_2\text{CO}_3$ carbothermal reduction regeneration process was designed, and after 200 cycles at 0.1C, regenerated LFP maintained a discharge specific capacity of 128.9 mA h g^{-1} , with a capacity retention rate of 90.77%. Economic evaluation shows that the cost of processing 1 kg of SLFP battery black powder is approximately USD 2.6255, a 41.2% reduction compared to traditional hydrometallurgical processes, while the process also decreases wastewater discharge by 76% [37,38]. This study provides a technically feasible and economically competitive solution for the high-value recycling of used LFP batteries, which contributes to the sustainable development of the lithium battery industry.

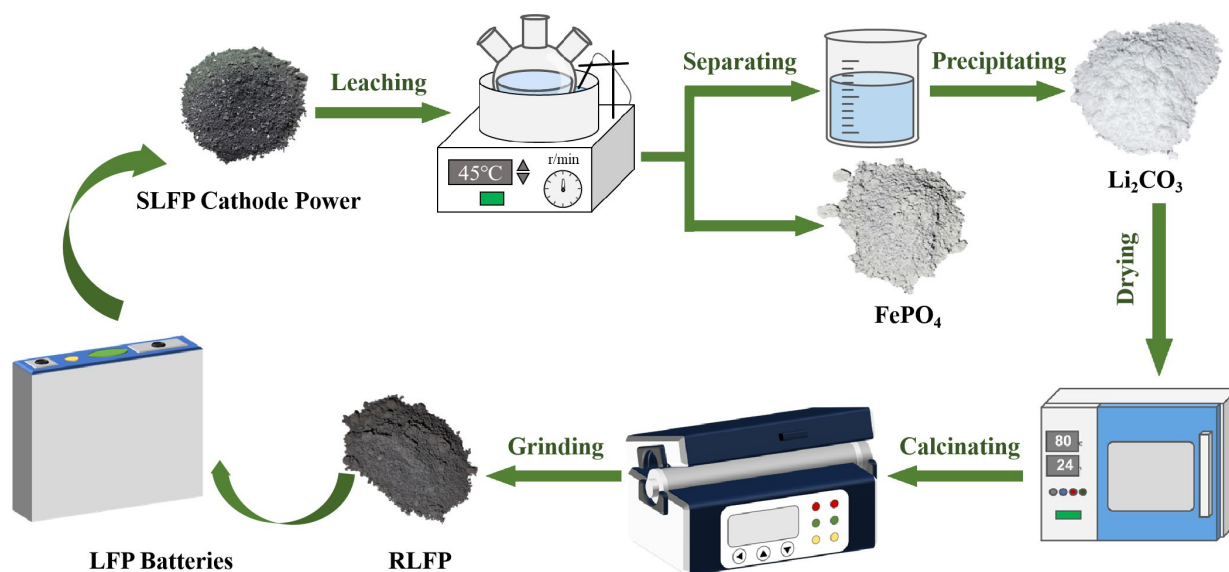


Figure 1. The short-process recycling system integrating “selective leaching, directional precipitation, and closed-loop regeneration”.

2. Results and Discussion

Figure 2a shows photographs of SLFP cathode powder before and after heat treatment. After heat treatment, the positive electrode material is easily peeled off the aluminum foil. The SEM image shows that the particles exhibit spherical morphology with a size of 0.17~1.31 μm (Figure 2b and Figure S1). The XRD pattern shown in Figure 2c displays diffraction angles at 35.591° , 25.561° , and 29.706° that correspond to the (311), (111), and (020) planes of crystalline LiFePO_4 (PDF#04-010-3115), respectively. Figure 2d demonstrates that the elemental content of SLFP was 35.35% Fe, 4.43% Li, and 18.98% P. XPS was used to further study the surface element composition, and the Fe, O, C, P, and Li elements could be observed (Figure 2e).

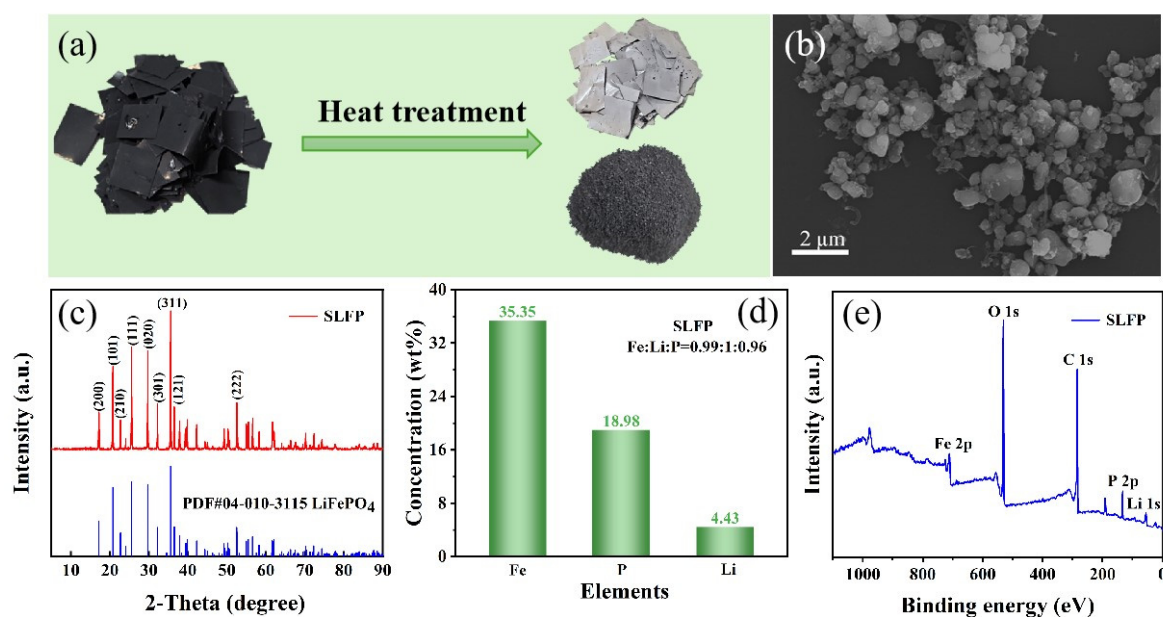


Figure 2. (a) Photographs of the SLFP cathode and the powder peeled off the aluminum foil, (b) the SEM images, (c) the XRD pattern, (d) the elemental content, and (e) the XPS spectra of SLFP cathode powder.

The effect of different variables including the sulfuric acid concentration, $\text{H}_2\text{SO}_4/\text{Li}$ molar ratio, leaching time, $\text{H}_2\text{O}_2/\text{Li}$ molar ratio, and leaching temperature on the leaching rates of Li and Fe in SLFP was investigated.

Sulfuric acid has been widely used as a leaching agent in the recycling of spent lithium-ion batteries. Traditional hydrometallurgical processes often employ excessive and high concentrations of H_2SO_4 to ensure complete metal leaching, but this method suffers from high reagent costs, complex subsequent processing, and significant wastewater discharge [39–42]. To find a local optimum within the considered experimental domain, the effect of H_2SO_4 concentration (0.1–1.9 M) on metal leaching behavior was systematically investigated under fixed conditions: $\text{H}_2\text{SO}_4/\text{Li}$ molar ratio of 0.55, $\text{H}_2\text{O}_2/\text{Li}$ molar ratio of 2.07, leaching temperature of 60 °C and time of 120 min, and stirring rate of 500 rpm. The experimental results (Figure 3a) show that Li exhibited highly selective leaching in the H_2SO_4 concentration range of 0.1–0.9 M, with its leaching efficiency significantly increasing from 78.38% to 97.13%, while the leaching efficiency of Fe remained below 0.5%. Notably, when the H_2SO_4 concentration exceeded 0.9 M, the leaching efficiency of Fe increased sharply from 0.21% to 2.86%, while the leaching efficiency of Li remained stable. Based on the selective leaching performance and economic considerations, 0.9 M was selected as the preferred H_2SO_4 concentration within the tested domain.

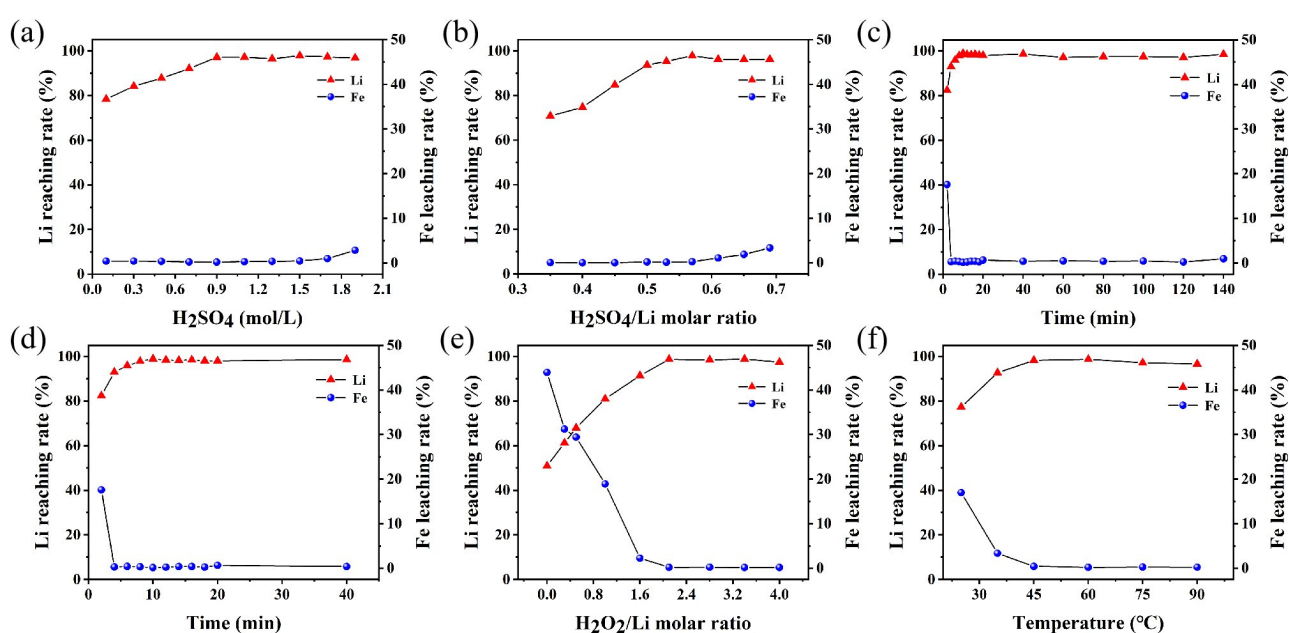
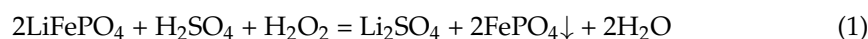


Figure 3. Influence of leaching conditions on leaching rates of Li and Fe. (a) Sulfuric acid concentration, (b) $\text{H}_2\text{SO}_4/\text{Li}$ molar ratio, (c) leaching time, (d) leaching time within first 45 min, (e) $\text{H}_2\text{O}_2/\text{Li}$ molar ratio, and (f) reaction temperature.

The mechanism of selective lithium extraction in the $\text{H}_2\text{SO}_4\text{-H}_2\text{O}_2$ system can be described by Equation (1):



In this reaction, H_2O_2 acts as an oxidant to elevate the redox potential (ORP) of the solution, promoting the oxidation of Fe^{2+} to Fe^{3+} . Under appropriate ORP conditions, Fe^{3+} rapidly reacts with PO_4^{3-} to form insoluble FePO_4 , effectively suppressing Fe dissolution. Meanwhile, Li^+ is released into the solution as Li_2SO_4 . This ORP-driven selectivity ensures that Fe remains in the solid phase while Li is leached efficiently. The ORP value is optimized by adjusting the $\text{H}_2\text{O}_2/\text{Li}$ molar ratio.

To investigate the effect of H_2SO_4 on the leaching rates of Li and Fe, experiments were conducted at $60\text{ }^\circ\text{C}$ and 500 rpm using 0.9 M H_2SO_4 , with a $\text{H}_2\text{O}_2/\text{Li}$ molar ratio of 2.07 and a reaction time of 120 min. The experimental results are shown in Figure 3b. When the $\text{H}_2\text{SO}_4/\text{Li}$ molar ratio increased from 0.35 to 0.57, the Li leaching rate significantly improved to 97.83%, while the Fe leaching rate remained below 0.3%. However, as the $\text{H}_2\text{SO}_4/\text{Li}$ molar ratio further increased to 0.57–0.69, the Li leaching rate stabilized, whereas the Fe leaching rate continued to rise, reaching 3.31%. This indicates that excessive H_2SO_4 not only fails to enhance Li leaching but also dissolves some FePO_4 , leading to an increase in Fe leaching. Therefore, a $\text{H}_2\text{SO}_4/\text{Li}$ molar ratio of 0.57 is appropriate.

Under the conditions of 0.9 M H_2SO_4 , a $\text{H}_2\text{SO}_4/\text{Li}$ molar ratio of 0.57, a $\text{H}_2\text{O}_2/\text{Li}$ molar ratio of 2.07, a leaching temperature of $60\text{ }^\circ\text{C}$, and a stirring speed of 500 rpm, the effects of different reaction times ranging from 2 to 140 min on the leaching rates of Li and Fe were investigated. As shown in Figure 3c,d, after 2 min of reaction, the leaching rates of Li and Fe were 82.39% and 17.59%, respectively. With prolonged reaction time, the Li leaching rate gradually increased, reaching a peak of 98.90% at 10 min, while the Fe leaching rate decreased to 0.1621%. Further extension of the reaction time had minimal impact on the leaching rates of Li and Fe. Considering economic efficiency, the appropriate leaching time was determined to be 10 min.

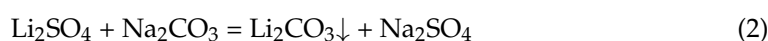
Under the conditions of 0.9 M H_2SO_4 , a $\text{H}_2\text{SO}_4/\text{Li}$ molar ratio of 0.57, a leaching time of 10 min, a leaching temperature of $60\text{ }^\circ\text{C}$, and a stirring speed of 500 rpm, the effects of different $\text{H}_2\text{O}_2/\text{Li}$ molar ratios on the leaching rates of Li and Fe were investigated. The results indicate that the reaction exhibits high selectivity upon the addition of H_2O_2 (Figure 3e). As the $\text{H}_2\text{O}_2/\text{Li}$ molar ratio increases, the Li leaching rate rises rapidly and then stabilizes, while the Fe leaching rate shows the opposite trend. H_2O_2 acts as an oxidant, converting Fe^{2+} to Fe^{3+} , thereby forming Li_2SO_4 and FePO_4 . When the $\text{H}_2\text{O}_2/\text{Li}$ molar ratio reaches 2.1, the leaching rates of Li and Fe reach 98.72% and 0.219%, respectively, entering a stable phase. Further increasing the amount of H_2O_2 not only intensifies the reaction but also has limited effect on improving the Li leaching rate or reducing the Fe leaching rate. Therefore, a $\text{H}_2\text{O}_2/\text{Li}$ molar ratio of 2.1 was selected for subsequent experiments.

The effect of temperature ranging from $25\text{ }^\circ\text{C}$ to $90\text{ }^\circ\text{C}$ on leaching efficiency was investigated under the conditions of 0.9 M H_2SO_4 , a $\text{H}_2\text{SO}_4/\text{Li}$ molar ratio of 0.57, a $\text{H}_2\text{O}_2/\text{Li}$ molar ratio of 2.1, a leaching time of 10 min, and a stirring speed of 500 rpm. The experimental results (Figure 3f) show that at $25\text{ }^\circ\text{C}$, the Li leaching rate was 77.29%, while the Fe leaching rate reached 16.96%. Increasing the temperature significantly enhanced the molecular energy of the reactants and reduced the activation energy, thereby accelerating the reaction process of Equation (1). Meanwhile, as the dissolution process of FePO_4 in water is an exothermic reaction, the solubility of FePO_4 decreases as the temperature rises, which further reduces the leaching of iron. At $45\text{ }^\circ\text{C}$, the Li leaching rate increased to 98.27%, while the Fe leaching rate decreased to 0.4306%. Further increasing the temperature resulted in a slight improvement in the Li leaching rate and a minor decrease in the Fe leaching rate, but the changes were limited. Considering both the leaching efficiency and energy consumption, $45\text{ }^\circ\text{C}$ was determined to be the appropriate reaction temperature.

Therefore, the local optimal conditions based on the OVAT method are as follows: the concentration of H_2SO_4 is 0.9 M, the molar ratio of $\text{H}_2\text{SO}_4/\text{Li}$ is 0.57, the molar ratio of $\text{H}_2\text{O}_2/\text{Li}$ is 2.1, the leaching time is 10 min, the temperature is $45\text{ }^\circ\text{C}$, and the stirring speed is 500 rpm. At this time, the solid–liquid ratio is 186.9 g/L, which is much higher than the 100 g/L of the traditional process [34]. We collated the relevant literature and made comparisons in terms of the leaching rate, leaching conditions, products, advantages and limitations, etc. For details, please refer to Table S1.

After purification and concentration, the leaching solution was treated with Na_2CO_3 to precipitate and recover Li in the form of Li_2CO_3 . The leaching solution was obtained under local optimal conditions (0.9 M H_2SO_4 , $\text{H}_2\text{SO}_4/\text{Li}$ molar ratio of 0.57, $\text{H}_2\text{O}_2/\text{Li}$ molar ratio of 2.1, leaching time of 10 min, temperature of 45 °C, and stirring speed of 500 rpm), and the impurities were removed by adjusting the pH with a NaOH solution. Then the obtained solution was concentrated to different concentrations, and the subsequent precipitation experiment was carried out at 95 °C for 15 min.

Figure S2a–e show the influence of Na_2CO_3 addition on the Li precipitation rate at different Li concentrations. When the Li concentration was 2 g L^{-1} , no Li_2CO_3 precipitation was observed. When the concentration of Li concentration increased to 10 g L^{-1} , with the addition of stoichiometric Na_2CO_3 , the precipitation rate of Li was 59.21% (Equation (2)). When the concentration was further increased to 25 g L^{-1} , the stoichiometric Na_2CO_3 addition achieved a Li precipitation rate of 90.77%. Excess Na_2CO_3 did not significantly improve the precipitation rate, so the appropriate conditions were determined to be concentrating the leaching solution to 25 g L^{-1} .



The XRD pattern (Figure S3) indicates that the obtained Li_2CO_3 matches well with the standard card (PDF#97-010-0324), and no visible characteristic peaks of other phases are observed, indicating that the lithium of SLFP can be recycled as Li_2CO_3 . Figure S4 shows the photo and microstructure of the recovered Li_2CO_3 . It presents white crystals and a layered stacking structure with a size of 0.38–1.22 μm .

To study the reaction mechanism for the recovery of Li from SLFP via a selective leaching $\text{H}_2\text{SO}_4\text{-H}_2\text{O}_2$ system and H_2O_2 , a series of characterization studies of the products from the leaching process was carried out. The XRD pattern of the leaching residue (LR) is in good agreement with the standard card (PDF#97-009-2199), and no other peaks are found, indicating that Fe is recovered in the form of high-purity FePO_4 (Figure 4a).

The FT-IR spectrum of the LR is shown in Figure 4b. The characteristic peak band of the FePO_4 olivine structure was clearly observed at 1238.29 cm^{-1} [43]. This change in the valence state of Fe during the leaching process led to a slight shift in the vibration frequencies of the FT-IR spectrum. The stretching vibration bands corresponding to PO_4^{3-} shifted from 967.5 cm^{-1} and 1055.14 cm^{-1} to 957.26 cm^{-1} and 1020.36 cm^{-1} , respectively. The stretching vibration bands corresponding to octahedral FeO_6 shifted to 657.52 and 684.04 cm^{-1} [44]. The peaks corresponding to the PO_4 tetrahedron moved from 578.16 cm^{-1} and 549.88 cm^{-1} to 576.56 cm^{-1} and 532.82 cm^{-1} [45]. Additionally, the peak bands at 502.32 cm^{-1} and 469.4 cm^{-1} were related to the movement of Li^+ , and their intensities weakened as Li^+ was stripped from SLFP [46].

XPS was used to study the valence state changes in elemental iron during the leaching process (Figure 4c). As shown in Figure 4d, the characteristic Fe^{2+} peaks in the SLFP appeared at 710.8 eV and 723.9 eV in the $\text{Fe } 2p_{3/2}$ and $\text{Fe } 2p_{1/2}$ regions, respectively. In the XPS spectrum of the LR, the peaks at 711.9 eV and 725 eV in the $2p_{3/2}$ and $2p_{1/2}$ regions, respectively, were the characteristic peaks of Fe^{3+} , and no Fe^{2+} peaks were detected. This indicates that almost all the Fe^{2+} in SLFP was oxidized to Fe^{3+} in the LR. Compared with SLFP, the P 2p high-resolution XPS spectrum of the LR showed no significant change (Figure S5). The C 1S spectrum of the LR (Figure S6) revealed the characteristic peak of C=O/O-C=O , which indicates that a certain amount of carbon had undergone oxidation.

Figure 4e shows the SEM image of the LR. The particle size of the LR (Figure S7) is smaller than that of SLFP due to Li release, and the spherical particle size is relatively homogeneous. The characterization tests indicate that SLFP is directly converted to the olivine structure of FePO_4 via an in situ reaction. The corresponding element mapping

image (Figure 4f) shows that the Fe, P, and O elements are evenly distributed throughout the selected area. In addition, a small amount of the element C is detected, which may be derived from the remaining conductive agent in the LFP electrode residue.

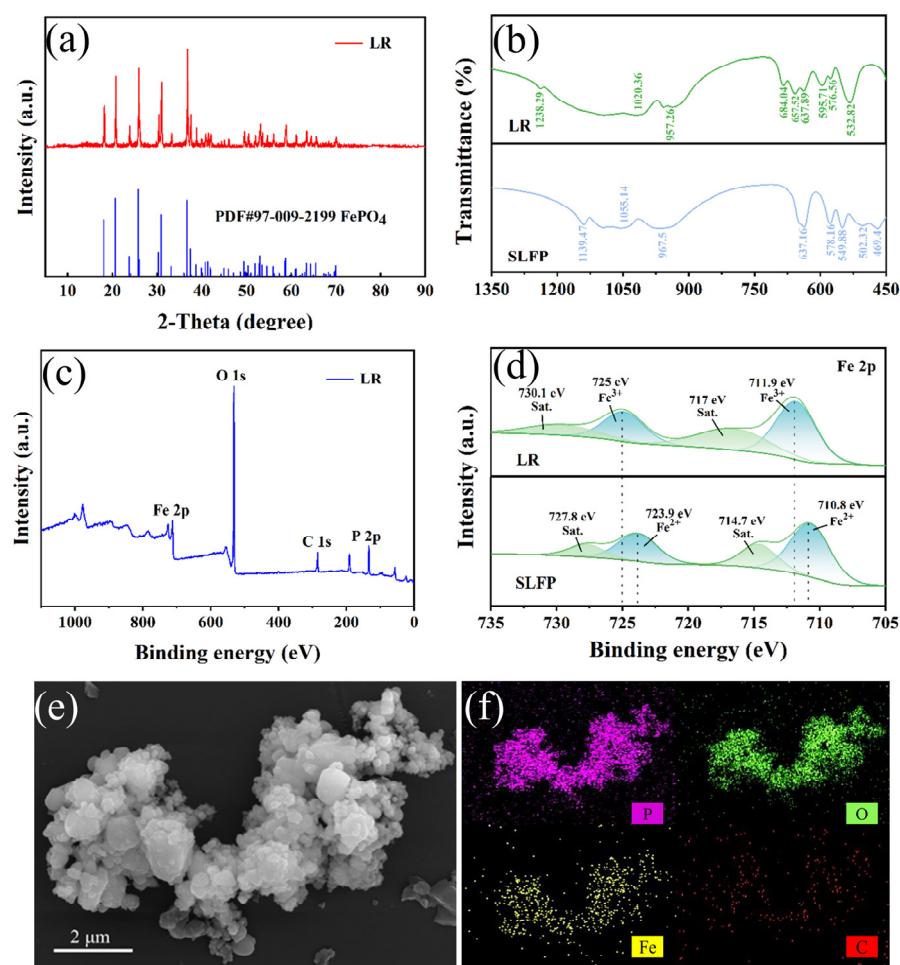


Figure 4. (a) XRD pattern of LR, (b) FT-IR spectra of LR and SLFP, (c) XPS spectra of LR, (d) Fe 2p spectra of LR and SLFP, (e) SEM image of LR, and (f) elemental mapping of LR.

Figure 5a shows the SEM image of regenerated lithium iron phosphate (RLFP), exhibiting spherical morphology with a size of 0.19~1.23 μm (Figure S8), similar to commercial lithium iron phosphate (CLFP) (Figure S9). The smaller size is conducive to enhancing the mobility of Li^+ , reducing the interface resistance and polarization of the electrode electrolyte, and thus improving electrochemical performance. The XRD patterns of SLFP and RLFP are shown in Figure 5b. The peak intensity of RLFP is weaker than that of SLFP, which indicates that there is a defect in the crystallinity of RLFP. It is consistent with the standard LFP card (PDF#04-010-3115), and no impurities were detected.

To further demonstrate the feasibility of the closed-loop process, half cells of R-LFP and CLFP were assembled separately, and their electrochemical properties were tested. As shown in Figure 5c, the first discharge capacity of RLFP is 124.5 mA h g^{-1} , slightly lower than that of CLFP (142.3 mA h g^{-1}).

At rates of 0.1C, 0.2C, 0.5C, 1C, and 2C, the initial discharge specific capacities of RLFP are 123.6, 132.6, 126.5, 117.4, and 74.1 mA h g^{-1} , respectively, lower than those of CLFP (139.1, 144.1, 136.4, 127, and 91.8 mA h g^{-1}) (Figure 5d,e), which may be related to trace impurities in the recycled material. At a rate of 0.1C, the discharge capacity of RLFP reaches 92.96% of that of CLFP after the 20th cycle. However, at a 2C rate, the capacity of RLFP

after the 20th cycle is only 79.10% of that of CLFP, indicating that capacity decay occurs more rapidly under high-current conditions. When the rate is reduced to 0.1C, the capacity of RLFP recovers to $134.8 \text{ mA h g}^{-1}$, confirming good electrochemical reversibility and structural stability.

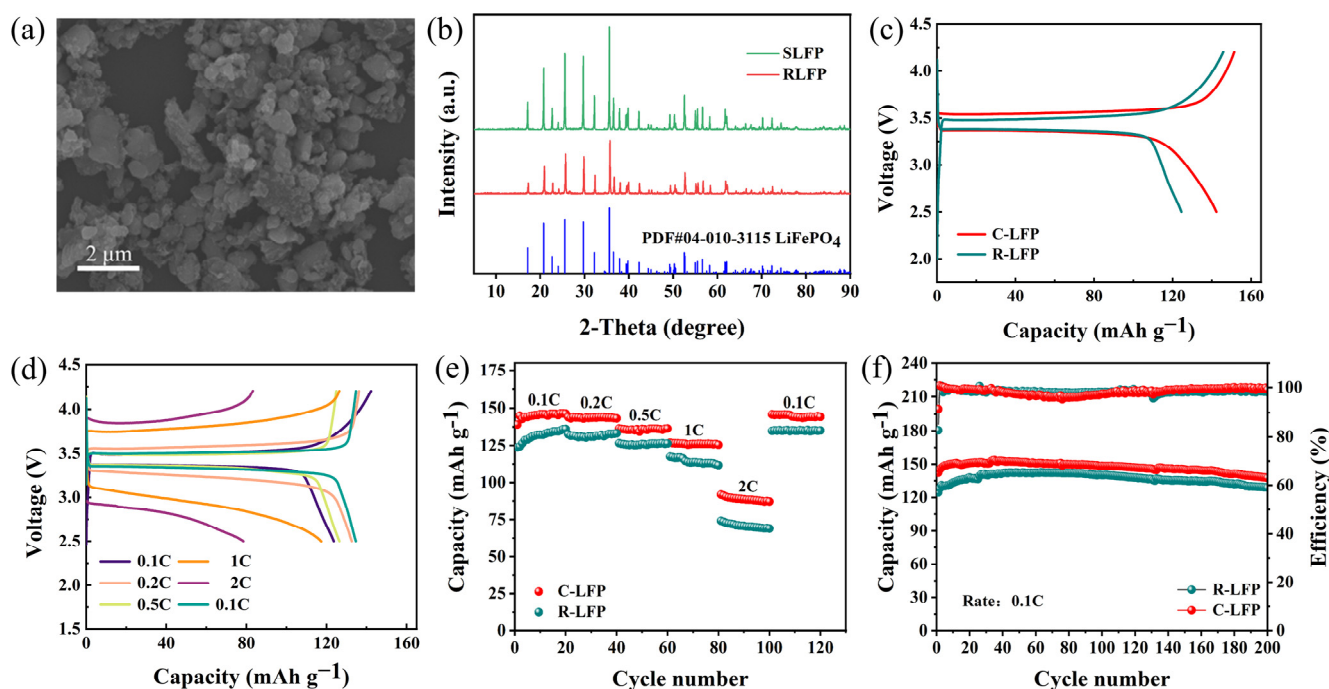


Figure 5. (a) SEM image of RLFP, (b) XRD patterns of RLFP and SLFP, (c) initial charge–discharge profiles of RLFP and CLFP at 0.1C, (d) initial charge–discharge curves of RLFP at different rates, (e) rate capability of RLFP and CLFP, and (f) cycling performance of RLFP and CLFP at 0.1C.

More importantly, after 200 cycles at 0.1C, RLFP maintained a discharge specific capacity of $128.9 \text{ mA h g}^{-1}$, with a capacity retention rate of 90.77%; the material maintains relatively stable capacity during cycling (Figure 5f). Overall, the short-process recycling process collects high-purity Li_2CO_3 and uses the leaching products to regenerate a LiFePO_4 cathode with good electrochemical properties, forming a sustainable closed loop.

Based on the experimental data in Figure 3 and Table 1, we conducted a preliminary assessment of the costs associated with the developed process. The cost references for chemicals (such as H_2SO_4 and H_2O_2), electricity, etc., are shown in Table S2. The cost of processing 1 kg of SLFP battery black powder is approximately USD 2.6255, while the value of the RLFP product is USD 4.4550, contributing the majority of the profit (Table S3). The product value is sufficient to cover the costs of chemicals and electricity. Furthermore, with the potential rebound in LFP prices and the cost reductions achievable through scaling up production, profits are expected to increase further. The process has the characteristics of low chemical and energy consumption, simplicity, the good electrochemical performance of the product, and the amount of acid used being basically less than in others, demonstrating that it is not only in line with the concept of green production but also has the advantage of environmental protection, which shows the great potential of SLFP battery recycling. Future work should focus on a more precise evaluation of economic and environmental benefits based on pilot-scale laboratory tests, including considerations of labor costs, equipment maintenance, and waste treatment expenses.

Table 1. Experimental input, energy consumption, and waste per batch (one batch is 1.0 kg black powder).

Materials	Amount per Batch	Cost Per Ton (USD) Market Price in China in 2024	Cost Per Batch (USD)
Waste LFP battery black powder (kg)	1.0	1390.1	1.3901
H ₂ SO ₄ (L)	0.196	37.14	0.0073
Leaching water (L)	5.154	0.41	0.0021
Washing water (L)	3.165	0.41	0.0013
H ₂ O ₂ (L)	1.343	112.90	0.1516
NaOH (kg)	0.032	372.33	0.0119
Na ₂ CO ₃ (kg)	0.332	273.51	0.0908
Glucose (kg)	0.227	345.18	0.0784
N ₂ (L)	5.400	61.85	0.3340
Electricity		0.107/KW h	0.5580
Leaching–heating/stirring (KW h)	0.222		
Leaching–filtration/drying (KW h)	0.650		
Calcination of filter residue (KW h)	0.410		
Precipitation–evaporation (KW h)	0.143		
Precipitation–drying (KW h)	0.650		
Ball milling (KW h)	1.380		
Synthetic calcination (KW h)	1.760		
Total electricity calculation (KW h)	5.215		
Total			2.6255

3. Experimental Section

3.1. Materials and Pretreatment

The spent LFP batteries used in this study were supplied by EVE Energy Co., Ltd. (Huizhou, China). All chemical reagents, including H₂SO₄, H₂O₂, Na₂CO₃, NaOH, and glucose, were of analytical grade and obtained from Sinopharm Chemical Reagent Co., Ltd. (Shanghai, China). The solutions used in this experiment were prepared with ultrapure water (resistivity: 18.2 MΩ·cm, UPT-II-20T, Ulupure Technology Co., Ltd., Chengdu, China).

The positive electrode pieces were first cut into small pieces, and then the small pieces were placed in a tube furnace and heat-treated at 500 °C in an argon atmosphere for 30 min. Finally, the waste LFP cathode powder was obtained by peeling off the aluminum foil. The cathode powder was treated using the wet acid digestion method. First, 0.1 g powder was added to a beaker, followed by an appropriate amount of concentrated hydrochloric acid, and then reacted at 70 °C for a specified duration. After digestion, a clarified solution was obtained, which was then diluted and used for further analysis.

3.2. Instrumentation and Analysis Method

The elemental content in the solution was determined using an inductively coupled plasma optical emission spectrometer (ICP-OES, Agilent 5800, Agilent Technologies Inc., Santa Clara, CA, USA); both Li and Fe adopted the radial view mode. The composition and structure of the samples were analyzed using an X-ray diffraction (XRD) instrument (Smart Lab 3KW, Rigaku Corporation, Akishima, Japan); the morphology of the solid particles was observed using a scanning electron microscope (SEM, JSM-6390LV, Japan Electronics Co., Ltd., Akishima, Japan); and the distribution of elements in the products was analyzed using an energy-dispersive spectrometer (EDS, X-Max^N 80T, Oxford Instruments, Abingdon-on-Thames, UK). Changes in the chemical valence states of the elements during leaching were studied using an X-ray photoelectron spectroscopy analyzer (XPS, K-Alpha X, Thermo Fisher Scientific, Waltham, MA, USA). The molecular structure was identified by a Fourier-transform infrared spectrometer (FTIR, IRTracer-100, Shimadzu Corporation, Kyoto, Japan).

3.3. Leaching and Resynthesis Processes

The leaching parameters were studied using the One Variable at a Time (OVAT) method. This means that what is found within the considered experimental domain is the local optimal value rather than the true global optimal value. The leaching of the cathode material is typically conducted in a 250 mL three-necked flask. First, 3.16 g cathode material was mixed with varying amounts of H_2SO_4 and H_2O_2 , with a constant stirring speed of 500 rpm maintained throughout the leaching experiments. After the reaction was complete, the mixture was filtered. The filtrate was then diluted to an appropriate concentration before being analyzed using ICP-OES. The leaching rate of each element was determined using the following Equation (3):

$$X_{\theta} = \frac{C_{\theta} \times V}{m \times W_{\theta}} \times 100\% \quad (3)$$

In the equation, C_{θ} (g/L) and V (L) represent the concentration of element θ in the filtrate and the volume of the filtrate solution, respectively. m (g) and W_{θ} represent the mass of the cathode material and the mass fraction of element θ in the cathode material, respectively. The filtrate obtained after leaching was used to adjust the pH with 10 wt% NaOH solution to precipitate trace amounts of iron and aluminum, and then it was evaporated and concentrated to obtain a solution with a specific lithium-ion concentration. At 95 °C, Na_2CO_3 was introduced and allowed to react for a designated period, resulting in the formation of a white precipitate. The mixture was filtered, and the filter residue was washed with boiling ultrapure water, dried to constant weight, and ground to yield Li_2CO_3 . The post-leaching filter residue was dried and calcined in a tubular furnace at 600 °C under an air atmosphere for 4 h to remove residual carbon, followed by grinding to produce FePO_4 . Finally, LiFePO_4/C was synthesized via a carbothermal reduction method using the recovered Li_2CO_3 and FePO_4 as raw materials in a Li:Fe:P molar ratio of 1.05:1:1. Glucose (20 wt%) served as the carbon source to reduce Fe^{3+} to Fe^{2+} , while simultaneously forming a continuous carbon network through thermal decomposition, thereby enhancing electrical conductivity.

4. Conclusions

This study developed a closed-loop process for the rapid and selective extraction of lithium from SLFP batteries, followed by resynthesis, demonstrating both economic viability and high efficiency. The process employs a selective leaching H_2SO_4 - H_2O_2 system, achieving highly selective lithium leaching (with a leaching rate of 98.72%) and efficient recovery of FePO_4 , while controlling the iron leaching rate at just 0.219%. Through an exploration of the precipitation conditions of the lithium-containing solution, high-purity Li_2CO_3 was obtained, which was then combined with FePO_4 through a carbothermal reduction process to synthesize a new LFP cathode. Preliminary economic assessments indicate that the cost of processing one kilogram of SLFP battery black powder is approximately USD 2.6255, while the value of RLFP reaches USD 4.455, highlighting significant economic benefits. In addition, very little acid is used in the process, indicating an advantage in terms of environmental protection.

Although the OVAT method effectively reduces the actual operation parameters, it is ultimately not globally optimal. Future optimizations based on Design of Experiments (DoE) can further improve this process. Although the process shows promising potential at the laboratory scale, further optimization is needed to address challenges in industrial-scale application, including the precise control of reaction conditions, equipment costs, and energy consumption in large-scale production. Moreover, the preliminary economic

assessment did not account for labor, equipment maintenance, or waste treatment costs, necessitating a more comprehensive analysis.

Supplementary Materials: The following supporting information can be downloaded at: <https://www.mdpi.com/article/10.3390/molecules30122587/s1>, Figure S1. The particle size distribution of SLFP; Figure S2. The influence of Na₂CO₃ addition on the Li precipitation rate at different Li concentrations: (a) 2g/L, (b) 10g/L, (c) 15g/L, (d) 20g/L, (e) 25g/L; Figure S3. XRD pattern of the obtained Li₂CO₃ precipitation recovered from SLFP; Figure S4. The photo (a), SEM image (b) and particle size distribution (c) of the recovered Li₂CO₃ precipitation recovered from SLFP; Figure S5. XPS spectra of P 2p: (a) SLFP, (b) LR; Figure S6. XPS spectra of C 1s: (c) SLFP, (d) LR; Figure S7. The particle size distribution of LR; Figure S8. The particle size distribution of RLFP; Figure S9. The SEM image (a) and the particle size distribution (b) of CLFP; Table S1. Comparison of the relevant literature on the selective leaching of LFP cathode materials; Table S2. Reference sources for parameter costs; Table S3. Cost and net product value for one batch experiment. References [47–52] are cited in the supplementary materials.

Author Contributions: Conceptualization, R.L. and Y.L.; Methodology, R.L. and Y.L.; Formal analysis, R.L., Y.L., and Y.C.; Investigation, Y.L., Y.C., and L.D.; Data curation, Y.L., Y.C., Y.Z., and K.Z.; Writing—original draft, Y.L. and S.Z.; Writing—review and editing, X.Z., J.L., and L.Z.; Visualization, X.Z. and J.L.; Supervision, L.D.; Funding acquisition, R.L. All authors have read and agreed to the published version of the manuscript.

Funding: This work was financially supported by the Project “Development of Valuable Metal Recovery Process for Cathode of Waste Lithium Iron Phosphate Battery” (RH2300001587).

Data Availability Statement: Data are contained within the article and Supplementary Materials.

Conflicts of Interest: The authors declare no conflicts of interest. The funders had no role in the design of the study; in the collection, analyses or interpretation of the data; in the writing of the manuscript; or in the decision to publish the results.

References

1. Bai, X.; Sun, Y.; Li, X.; He, R.; Liu, Z.; Pan, J.; Zhang, J. A Deep Dive into Spent Lithium-Ion Batteries: From Degradation Diagnostics to Sustainable Material Recovery. *Electrochem. Energy Rev.* **2024**, *7*, 33. [[CrossRef](#)]
2. Shi, P.; Jie, Y.; Hu, F.; Yang, S.; Chang, D.; Fang, G.; Ding, J.; Qu, X.; Wu, G.; Zhu, H.; et al. From Waste to Material Strategy: A Closed-Loop Regeneration Process of Spent LiFePO₄ Batteries. *Sep. Purif. Technol.* **2025**, *359*, 130502. [[CrossRef](#)]
3. Lin, J.; Zhang, X.; Fan, E.; Chen, R.; Wu, F.; Li, L. Carbon Neutrality Strategies for Sustainable Batteries: From Structure, Recycling, and Properties to Applications. *Energy Environ. Sci.* **2023**, *16*, 745–791. [[CrossRef](#)]
4. Chacko, B.; Madhuri, W. A Comprehensive Investigation on the Electrochemical Performance, Synthesis, Modification, and Recycling Methods of LiFePO₄ for Sustainable Future. *J. Energy Storage* **2024**, *98*, 112851. [[CrossRef](#)]
5. Rostami, H.; Valio, J.; Tynjala, P.; Lassi, U.; Suominen, P. Life Cycle of LiFePO₄ Batteries: Production, Recycling, and Market Trends. *ChemPhysChem* **2024**, *25*, e202400459. [[CrossRef](#)]
6. Zhang, M.; Wang, L.; Wang, S.; Ma, T.; Jia, F.; Zhan, C. A Critical Review on the Recycling Strategy of Lithium Iron Phosphate from Electric Vehicles. *Small Methods* **2023**, *7*, 2300125. [[CrossRef](#)]
7. Mordor Intelligence. Available online: <https://www.mordorintelligence.com/industry-reports/lfp-battery-pack-market> (accessed on 25 March 2025).
8. Li, G.; Chen, Y.; Wu, M.; Xu, Y.; Li, X.; Tian, M. High-Efficiency Leaching Process for Selective Leaching of Lithium from Spent Lithium Iron Phosphate. *Waste Manag.* **2024**, *190*, 141–148. [[CrossRef](#)]
9. Jiang, Y.; Peng, C.; Zhou, K.; Zhou, H.; Chen, T.; Zhang, G.; Chen, W. Impact and Removal of Fluorine Impurity in the Comprehensive Recovery of Spent LiFePO₄/C. *Sep. Purif. Technol.* **2025**, *362*, 131766. [[CrossRef](#)]
10. Wang, Y.; Goikolea, E.; De Larramendi, I.R.; Lanceros-Méndez, S.; Zhang, Q. Recycling Methods for Different Cathode Chemistries—A Critical Review. *J. Energy Storage* **2022**, *56*, 106053. [[CrossRef](#)]
11. Zeng, Z.; Lei, H.; Lu, X.; Zhu, C.; Wen, Y.; Zhu, J.; Ji, X.; Sun, W.; Yang, Y.; Ge, P. Li-Fe Anti-Sites Defects in LiFePO₄: Mechanism, Characterization and Cathode-Regeneration Applications. *Energy Storage Mater.* **2025**, *74*, 103947. [[CrossRef](#)]

12. Fu, D.; Zhou, W.; Liu, J.; Zeng, S.; Wang, L.; Liu, W.; Yu, X.; Liu, X. A Facile Route for the Efficient Leaching, Recovery, and Regeneration of Lithium and Iron from Waste Lithium Iron Phosphate Cathode Materials. *Sep. Purif. Technol.* **2024**, *342*, 127069. [[CrossRef](#)]
13. Xie, J.; Xiao, S.; Xu, W.; Liu, D.; Ren, G. A Green and Simplified Method for Selective Recovery of Lithium from the Cathode Scraps of Spent $\text{LiFe}_x\text{Mn}_{1-x}\text{PO}_4$ Batteries. *Sep. Purif. Technol.* **2024**, *341*, 126848. [[CrossRef](#)]
14. Zhang, Y.; Wang, B.; Wang, F.; Dai, Y.; Ren, S.; Hou, Y.; Wu, W. A Green Recyclable Process for Selective Recovery of Li and Fe from Spent Lithium Iron Phosphate Batteries by Synergistic Effect of Deep Eutectic Solvent and Oxygen. *Sep. Purif. Technol.* **2025**, *354*, 128764. [[CrossRef](#)]
15. Ma, J.; Xu, Z.; Yao, T.; Chen, Z.; Liu, X.; Sun, Q.; Jin, Y.; Song, L.; Zhang, M.-D. A Method of Efficiently Regenerating Waste LiFePO_4 Cathode Material after Air Firing Treatment. *ACS Appl. Mater. Interfaces* **2024**, *16*, 65119–65130. [[CrossRef](#)]
16. Jing, C.; Tran, T.T.; Lee, M.S. A Review on the Recovery of Lithium and Iron from Spent Lithium Iron Phosphate Batteries. *Miner. Process. Extr. Metall. Rev.* **2024**, *45*, 892–903. [[CrossRef](#)]
17. Yan, Y.; Lv, Y.; Sun, Y.; Chen, M.; Zhou, D.; Sun, L.; Cheng, H.; Li, W.; Chen, Z.; Tang, C.-M.; et al. Green and Efficient Selective Lithium Extraction from Spent Lithium-Ion Batteries Using a Self-Pressurizing-Assisted Oxidative Fixation System. *Sep. Purif. Technol.* **2025**, *362*, 131716. [[CrossRef](#)]
18. Wen, G.; Yuan, S.; Dong, Z.; Gao, P.; Ding, H.; Lei, S.; Liu, Q. Mechanism and Process Study of Spent Lithium Iron Phosphate Batteries by Medium-Temperature Oxidation Roasting Strategy. *Sep. Purif. Technol.* **2025**, *356*, 129987. [[CrossRef](#)]
19. Wu, G.; Chen, H.; Wang, D.; Zhang, Y.; Xu, J. Chemistry Evolution of $\text{LiFePO}_4\text{-NaHSO}_4\cdot\text{H}_2\text{O}$ System during Roasting and Recovery of Li and Fe. *J. Alloys Compd.* **2024**, *1007*, 176376. [[CrossRef](#)]
20. Zhang, G.; Shi, M.; Hu, X.; Yang, H.; Yan, X. Comparison of Life Cycle Assessment of Different Recycling Methods for Decommissioned Lithium Iron Phosphate Batteries. *Sustain. Energy Technol. Assess.* **2024**, *68*, 103871. [[CrossRef](#)]
21. Yang, D.; Fang, Z.; Ji, Y.; Yang, Y.; Hou, J.; Zhang, Z.; Du, W.; Qi, X.; Zhu, Z.; Zhang, R.; et al. A Room-Temperature Lithium-Restocking Strategy for the Direct Reuse of Degraded LiFePO_4 Electrodes. *Angew. Chem.-Int. Ed.* **2024**, *63*, e202409929. [[CrossRef](#)]
22. Qiu, X.; Wang, C.; Liu, Y.; Han, Q.; Xie, L.; Zhu, L.; Cao, X. Ambient-Pressure Relithiation of Spent LiFePO_4 Using Alkaline Solutions Enables Direct Regeneration of Lithium-Ion Battery Cathodes. *J. Energy Storage* **2025**, *105*, 114721. [[CrossRef](#)]
23. Qiu, X.; Wang, C.; Xie, L.; Zhu, L.; Cao, X.; Ji, X. Challenges and Perspectives towards Direct Regeneration of Spent LiFePO_4 Cathode. *J. Power Sources* **2024**, *602*, 234365. [[CrossRef](#)]
24. Li, C.; Gong, R.; Zhang, Y.; Meng, Q.; Dong, P. Direct Regeneration of Degraded LiFePO_4 Cathode via Reductive Solution Relithiation Regeneration Process. *Molecules* **2024**, *29*, 3340. [[CrossRef](#)] [[PubMed](#)]
25. Song, S.; Liu, R.; Li, J.; Sun, W.; Yang, Y. Regeneration of LiFePO_4 from Spent Materials: Control and Influence of Al Impurity. *ChemSusChem* **2025**, *18*, e202401432. [[CrossRef](#)]
26. Niu, Y.; Shi, D.; Cheng, X.; Zhang, Y.; Li, L.; Song, F.; Xie, S.; Peng, X. A Closed-Loop Coupling Process of Leaching and Solvent Extraction for Li_2CO_3 and FePO_4 Recovery from Spent LiFePO_4 . *Sustain. Mater. Technol.* **2024**, *39*, e00827. [[CrossRef](#)]
27. Zhao, T.; Mahandra, H.; Choi, Y.; Li, W.; Zhang, Z.; Zhao, Z.; Chen, A. A Clean and Sustainable Method for Recycling of Lithium from Spent Lithium Iron Phosphate Battery Powder by Using Formic Acid and Oxygen. *Sci. Total Environ.* **2024**, *920*, 170930. [[CrossRef](#)]
28. Zhang, Q.; Fan, E.; Lin, J.; Sun, S.; Zhang, X.; Chen, R.; Wu, F.; Li, L. Acid-Free Mechanochemical Process to Enhance the Selective Recycling of Spent LiFePO_4 Batteries. *J. Hazard. Mater.* **2023**, *443*, 130160. [[CrossRef](#)]
29. Ali, M.; Iqbal, N.; Noor, T.; Zaman, N. Selective Lithium Recovery from Spent LFP Li-Ion Batteries Using Organic Acids. *Ionics* **2024**, *31*, 273–286. [[CrossRef](#)]
30. Wu, J.; Xiao, L.; Shen, L.; Ran, J.-J.; Zhong, H.; Zhu, Y.-R.; Chen, H. Recent Advancements in Hydrometallurgical Recycling Technologies of Spent Lithium-Ion Battery Cathode Materials. *Rare Met.* **2024**, *43*, 879–899. [[CrossRef](#)]
31. Luo, B.; Xu, B.; Yan, Q.; Zhou, Y.; Dong, Z.; Huang, X.; Zhao, Z. Advances and Challenges in Recycling Spent LiFePO_4 Batteries. *Sep. Purif. Technol.* **2025**, *362*, 131780. [[CrossRef](#)]
32. Qi, C.; Yao, T.; Zhai, W.; Zhang, M.; Song, L.; He, J. Advances in Degradation Mechanism and Sustainable Recycling of LiFePO_4 -Type Lithium-Ion Batteries. *Energy Storage Mater.* **2024**, *71*, 103623. [[CrossRef](#)]
33. Zeng, Y.; Wang, Y.; Cai, S.; Li, R.; Zhou, C.; Wang, C.; Ma, K.; Song, L.; Yue, H. All-Component Recycling and Reuse Process for Spent LiFePO_4 Cathodes. *Ind. Eng. Chem. Res.* **2024**, *63*, 6847–6856. [[CrossRef](#)]
34. Zheng, R.; Zhao, L.; Wang, W.; Liu, Y.; Ma, Q.; Mu, D.; Li, R.; Dai, C. Optimized Li and Fe Recovery from Spent Lithium-Ion Batteries via a Solution-Precipitation Method. *RSC Adv.* **2016**, *6*, 43613–43625. [[CrossRef](#)]
35. Liu, W.; Liu, M.; Ma, F.; Qin, M.; Zhong, W.; Chen, X.; Zeng, Z.; Cheng, S.; Xie, J. Direct Lithium Extraction from Spent Batteries for Efficient Lithium Recycling. *Sci. Bull.* **2024**, *69*, 1697–1705. [[CrossRef](#)]
36. Rao, S.; Zhang, T.; Wu, D.; Li, W.; Ma, Z.; Wang, D.; Zhu, W.; Liu, Z. Oxidation Pressure Leaching of Lithium Iron Phosphate: Kinetic Aspects, Leaching Mechanism, and the Behavior of Lithium and Iron. *J. Environ. Chem. Eng.* **2025**, *13*, 115658. [[CrossRef](#)]

37. Wu, Y.; Li, G.; Zhao, S.; Yin, Y.; Wang, B.; He, W. Selective Recovery of Lithium from Spent Lithium Iron Phosphate Batteries. *Waste Manag. Res.* **2024**. [[CrossRef](#)]
38. Li, Y.; Dong, L.; Shi, P.; Ren, Z.; Zhou, Z. Selective Recovery of Lithium from Lithium Iron Phosphate. *J. Power Sources* **2024**, *598*, 234158. [[CrossRef](#)]
39. Cui, K.; Zhao, M.-C.; Li, Y.; Atrens, A.; Zhang, F. Recycling of Spent Lithium Iron Phosphate Batteries: Research Progress Based on Environmental Protection and Sustainable Development Technology. *Sep. Purif. Technol.* **2025**, *354*, 128982. [[CrossRef](#)]
40. Jing, C.; Tran, T.T.; Lee, M.S. Recovery of Iron Phosphate and Lithium Carbonate from Sulfuric Acid Leaching Solutions of Spent LiFePO₄ Batteries by Chemical Precipitation. *Physicochem. Probl. Miner. Process.* **2024**, *60*, 189463. [[CrossRef](#)]
41. Wen, G.; Yuan, S.; Dong, Z.; Ding, H.; Gao, P. Recycling of Spent Lithium Iron Phosphate Battery Cathode Materials: A Review. *J. Clean. Prod.* **2024**, *474*, 143625. [[CrossRef](#)]
42. Hu, H.; Yao, Y.; Meng, X.; Li, Y.; Zhang, K.; Zhang, S.; Yang, Y.; Xu, Y.; Hu, J. Selective Lithium Recovery and Regeneration of LiFePO₄ from Spent Lithium-Ion Batteries: An Efficient and Green Process. *J. Power Sources* **2025**, *631*, 236179. [[CrossRef](#)]
43. Ait Salah, A.; Jozwiak, P.; Zaghbi, K.; Garbarczyk, J.; Gendron, F.; Mauger, A.; Julien, C.M. FTIR Features of Lithium-Iron Phosphates as Electrode Materials for Rechargeable Lithium Batteries. *Spectrochim. Acta Part A* **2006**, *65*, 1007–1013. [[CrossRef](#)]
44. Zhang, T.; Gong, D.; Lin, S.; Yu, J. Effect of pH-Dependent Intermediate on the Performance of LiFePO₄/C Cathode Material. *Chem. Eng. J.* **2022**, *449*, 137830. [[CrossRef](#)]
45. Yue, X.-H.; Zhang, C.-C.; Zhang, W.-B.; Wang, Y.; Zhang, F.-S. Recycling Phosphorus from Spent LiFePO₄ Battery for Multifunctional Slow-Release Fertilizer Preparation and Simultaneous Recovery of Lithium. *Chem. Eng. J.* **2021**, *426*, 131311. [[CrossRef](#)]
46. Jin, H.; Zhang, J.; Wang, D.; Jing, Q.; Chen, Y.; Wang, C. Facile and Efficient Recovery of Lithium from Spent LiFePO₄ Batteries via Air Oxidation–Water Leaching at Room Temperature. *Green Chem.* **2022**, *24*, 152–162. [[CrossRef](#)]
47. Li, H.; Xing, S.; Liu, Y.; Li, F.; Guo, H.; Kuang, G. Recovery of Lithium, Iron, and Phosphorus from Spent LiFePO₄ Batteries Using Stoichiometric Sulfuric Acid Leaching System. *ACS Sustain. Chem. Eng.* **2017**, *5*, 8017–8024. [[CrossRef](#)]
48. Chen, X.; Yuan, L.; Yan, S.; Ma, X. Self-Activation of Ferro-Chemistry Based Advanced Oxidation Process towards in-Situ Recycling of Spent LiFePO₄ Batteries. *Chem. Eng. J.* **2023**, *471*, 144343. [[CrossRef](#)]
49. Zhang, Z.; Tang, J.; Su, M.; Xu, J.; Shih, K. Design and Optimization of an Economically Viable and Highly Efficient Strategy for Li Recycling from Spent LiFePO₄ Batteries. *ACS Sustain. Chem. Eng.* **2023**, *11*, 16124–16132. [[CrossRef](#)]
50. Bruno, M.; Francia, C.; Fiore, S. Selective Leaching for the Recycling of Lithium, Iron, and Phosphorous from Lithium-Ion Battery Cathodes' Production Scraps. *Batteries* **2024**, *10*, 415. [[CrossRef](#)]
51. Gerold, E.; Lerchhammer, R.; Antrekowitsch, H. Parameter Study on the Recycling of LFP Cathode Material Using Hydrometallurgical Methods. *Metals* **2022**, *12*, 1706. [[CrossRef](#)]
52. Qin, X.; Yang, G.; Cai, F.; Wang, B.; Jiang, B.; Chen, H.; Tan, C. Recovery and Reuse of Spent LiFePO₄ Batteries. *J. New Mater. Electrochem. Syst.* **2019**, *22*, 119–124. [[CrossRef](#)]

Disclaimer/Publisher's Note: The statements, opinions and data contained in all publications are solely those of the individual author(s) and contributor(s) and not of MDPI and/or the editor(s). MDPI and/or the editor(s) disclaim responsibility for any injury to people or property resulting from any ideas, methods, instructions or products referred to in the content.